ceramics

MDPI

Article

Optimized Development of High-Porosity Structural and Thermal Insulation Foam Ceramics Based on Local Natural and Technogenic Raw Materials

Aidana Kuanyshbay [1], Sayat Niyetbay [1,2,*], Indira Tashmukhanbetova [1,*], Ruslanzhan Sadyrov [1], Nurgul Amangeldi [3], Laura Mustafa [4], Akmaral Nurakhova [5], Ilyas Rustemov [5] and Assel Yesbolat [5]

1 Faculty of General Construction, International Educational Corporation, Ryskulbekova Street, 28, Almaty 050043, Kazakhstan; a.kuanyshbay@mok.kz (A.K.); ru.sadyrov@mok.kz (R.S.)
2 Construction and Building Materials Department, Institute of Architecture and Civil Engineering, Satbayev University, 22 Satbayev Street, Almaty 050013, Kazakhstan
3 Faculty of Pre-University Education, Al Farabi Kazakh National University, Avenue Al—Farabi 71, Almaty 050040, Kazakhstan; nurgul.amangeldi@kaznu.edu.kz
4 National Center of Space Research and Technology, 15, Shevchenko St., Almaty 050010, Kazakhstan; l.mustafa@spaceres.kz
5 Department of "Transport Construction and Production of Building Materials", Kazakh Automobile and Road Institute Named After L.B. Goncharov, Raimbek Avenue, 415B, Almaty 050061, Kazakhstan; ay_ar77@mail.ru (A.N.); kipchak54@mail.ru (I.R.); ashkeyeva@mail.ru (A.Y.)
* Correspondence: s.nietbay@mok.kz (S.N.); i.tashmukhanbetova@mok.kz (I.T.)

Abstract: This study explores the optimization of foam ceramic materials through experimental research and mathematical modeling. The goal was to enhance mechanical strength, thermal insulation, porosity, water absorption, and density by adjusting composition and firing conditions. Regression analysis and response surface methodology were used to assess the effects of loam, fly ash content, and the firing temperature. The optimal composition of 60–65% loam, 10% fly ash, and a firing temperature of 950–1000 °C yielded foam ceramics with a bulk density of 680–700 kg/m^3, a compressive strength of 3.5–4 MPa, and a thermal conductivity of 0.135–0.140 W/(m·K). Controlled porosity (70–72%) enhanced insulation while maintaining structural integrity. X-ray diffraction confirmed mullite, quartz, and cristobalite phases, with mullite improving mechanical properties. This research demonstrates the potential of optimized foam ceramics for energy-efficient construction. Mathematical modeling and experimental validation provide a pathway for developing lightweight, high-performance ceramic materials. Future work should refine sintering processes, explore new additives, and evaluate the long-term performance.

Keywords: foam ceramics; optimization; mathematical modeling; thermal insulation; mechanical strength; porosity; water absorption

check for updates

Academic Editor: Malika Saadaoui

Received: 28 February 2025
Revised: 21 March 2025
Accepted: 26 March 2025
Published: 5 April 2025

Citation: Kuanyshbay, A.; Niyetbay, S.; Tashmukhanbetova, I.; Sadyrov, R.; Amangeldi, N.; Mustafa, L.; Nurakhova, A.; Rustemov, I.; Yesbolat, A. Optimized Development of High-Porosity Structural and Thermal Insulation Foam Ceramics Based on Local Natural and Technogenic Raw Materials. *Ceramics* **2025**, *8*, 35. https://doi.org/10.3390/ceramics8020035

Copyright: © 2025 by the authors. Licensee MDPI, Basel, Switzerland. This article is an open access article distributed under the terms and conditions of the Creative Commons Attribution (CC BY) license (https://creativecommons.org/licenses/by/4.0/).

1. Introduction

The demand for high-performance thermal insulation materials is increasing due to the necessity of improving energy efficiency in residential and industrial construction [1]. The necessity of improving energy efficiency in residential and industrial construction is increasingly evident, with the global energy demand for space heating and cooling accounting for approximately 35% of total building energy consumption. The adoption of advanced thermal insulation materials has been shown to reduce heat loss in buildings by up to 40%, significantly lowering energy costs and carbon emissions. Various materials, including dense and porous concrete, gypsum-based composites, and cellular ceramics, have

been developed to address these requirements. The ceramic industry still predominantly produces dense structural bricks with limited porosity, as evidenced by market reports indicating that over 80% of globally manufactured ceramic bricks fall within the category of dense structural ceramics with a porosity below 10% [1]. This trend highlights the need in construction for innovative porous ceramic materials to improve thermal insulation. However, despite the progress in building materials science, the ceramic industry still predominantly produces dense structural bricks with limited porosity, affecting their insulation properties. Granular foam glass, produced using recycled cullet and ceramic fillers, is an alternative lightweight insulating material. While it offers high compressive strength and resistance to chemical degradation, it has limitations in terms of thermal stability and brittleness compared to foam ceramics. In contrast, foam ceramics provide a more uniform pore structure, superior thermal insulation, and enhanced fire resistance, making them particularly suitable for high-temperature applications in construction. Recent studies have explored the possibility of producing granular foam glass using household and commercial cullet combined with ceramic fillers, demonstrating the feasibility of obtaining eco-friendly thermal insulation materials through controlled foaming techniques. These advancements highlight the potential of both materials in sustainable construction while emphasizing the advantages of foam ceramics in demanding thermal environments [2–7].

The heat-insulating properties of ceramic foams have made them widely applicable in high-temperature industrial settings, such as structural catalyst supports and energy storage systems. Research has shown that the effective thermal conductivity of ceramic foams is strongly influenced by the pore structure, stacking thickness, and temperature conditions [8–14]. Foam ceramics exhibit excellent heat-insulating properties due to their high porosity and low thermal conductivity, typically ranging from 0.05 to 0.15 W/(m·K) depending on the composition and processing conditions. Compared to conventional dense ceramics, these materials can reduce heat transfer by up to 50%, making them highly effective for energy-efficient building applications. These properties make them particularly valuable for applications requiring both thermal resistance and lightweight construction materials. Moreover, mathematical modeling and experimental validation play crucial roles in optimizing the physical and mechanical properties of foam ceramics [15]. Computational fluid dynamics (CFDs) simulations play a crucial role in optimizing the properties of foam ceramics by modeling heat transfer, pore structure evolution, and fluid behavior during foaming. These simulations enable the prediction of thermal conductivity, airflow resistance, and mechanical stability, allowing for the fine-tuning of processing parameters to achieve the desired porosity and insulation performance. By using CFD-based optimization, researchers can enhance the structural integrity and thermal efficiency of foam ceramics before conducting extensive experimental trials, reducing material waste and production costs. For instance, CFDs simulations have been used to evaluate the pressure drop in ceramic foam filters, providing insights into how the material structure influences fluid flow and heat transfer, further refining the design and functional performance of foam ceramics [16–23].

In Kazakhstan, extensive studies have been conducted on the thermal insulation performance of various construction materials, particularly by researchers such as Ibraimbayeva G.B., Orynbekov E.S., and Saduakasov M.D. These studies highlight the importance of developing innovative, eco-friendly insulation materials with enhanced mechanical and thermal properties. Kazakh researchers have actively explored the development of foam ceramics using local natural and industrial raw materials, focusing on optimizing the composition and processing conditions to improve their performance. Their findings align with the present study's focus on sustainable material development by demonstrating the feasibility of incorporating regional resources such as loess and fly ash into foam ceramics.

This synergy reinforces the global effort to create cost-effective, energy-efficient building materials whilst addressing local raw material availability and environmental concerns. Recent advancements in foam ceramic technology have focused on optimizing sintering conditions, where controlled heating rates and sintering times significantly affect the porosity, compressive strength, and water absorption of the final products. For instance, previous studies have shown that increasing the sintering temperature from 900 °C to 1100 °C can reduce the porosity from 85% to 65% whilst simultaneously increasing the compressive strength from 1.2 MPa to 4.5 MPa. Additionally, prolonged sintering times (e.g., from 60 to 180 min) can enhance densification but may lead to a decrease in the water absorption from 40% to 20%, depending on the composition of the ceramic mass [24–28]. Additionally, novel processing techniques for foam ceramics allow for the incorporation of industrial waste, such as coal gangue and phosphorus tailings, into their compositions, contributing to resource conservation and waste recycling.

Despite the progress in foam ceramic development, many conventional insulation materials, such as mineral wool and expanded polystyrene, have significant drawbacks. These include moisture sensitivity, fire hazards, and the release of toxic gases upon combustion. Alternative approaches, such as nanostructured foam ceramics, have demonstrated improved moisture resistance, mechanical strength, and chemical durability, making them a superior choice for long-term thermal insulation applications [29–36]. These materials, which undergo controlled sintering at temperatures between 950 and 1100 °C, exhibit high mechanical stability due to the formation of mullite-based crystal bonds within their microstructure.

Thus, the present study aims to explore the optimization of foam ceramic compositions based on local raw materials to achieve enhanced thermal insulation and mechanical properties. By evaluating the influence of key parameters such as foaming agents, the firing temperature, and the sintering conditions, this research seeks to optimize porosity, thermal conductivity, and compressive strength to improve the suitability of foam ceramics for modern construction applications. Refining the composition and processing conditions allows for an optimal balance between mechanical durability and thermal insulation efficiency. These improvements are particularly relevant for energy-efficient building materials, contributing to reduced heat loss, improved structural integrity, and sustainable resource utilization in construction.

2. Materials and Methods

The primary objective of technological experiments is to establish relationships that link the properties under investigation (such as strength, density, etc.) with a set of independent variables (such as additive content, drying time, and firing temperature). These relationships are used to optimize the process by identifying the best technological parameters.

Experimental planning plays a crucial role in mathematical modeling by minimizing the number of experiments while varying all influencing factors. Applying the principles of experimental theory enhances research efficiency, allowing researchers to construct mathematical models, optimize processes, and test various hypotheses with minimal resource expenditure. The range of tasks that experimental planning can address includes identifying optimal conditions, constructing interpolation formulas, evaluating and refining theoretical model constants, and studying composition–property relationships.

One of the most common scientific and technical challenges is determining the optimal conditions for a process once its feasibility has been established. This can be effectively approached using a cybernetic system model, often referred to as a “black box”, which Figure 1 schematically represents. The arrows on the right denote optimization parameters (y), which are also referred to as optimization criteria, objective functions, or black box outputs.



Figure 1. Black box diagram.

The primary objective of technological experiments is to establish relationships between investigated properties (e.g., strength, density) and independent variables (e.g., additive content, drying time, firing temperature) to optimize the process. Experimental planning plays a crucial role in minimizing the number of trials while systematically varying influencing factors. This approach enhances research efficiency by enabling the construction of mathematical models, the optimization of processes, and hypothesis testing with minimal resource expenditure.

Experimental planning addresses a wide range of tasks, including identifying optimal conditions, constructing interpolation formulas, refining theoretical model constants, and studying composition–property relationships. One of the most common challenges is determining optimal process conditions once feasibility has been established.

The research object can be represented using a cybernetic system model, often referred to as a "black box", as shown in Figure 1. The arrows denote optimization parameters (y), also known as optimization criteria or objective functions. To solve the research problem, mathematical models will be employed, where the response function links optimization parameters with influencing factors, as expressed in Equation (1) as follows:

$$y = f(x_1;x_2;x_3...x_n), \quad (1)$$

where f(x) represents the response function.

Various methods of mathematical planning are used in technological research, such as full factorial experiments (FFEs), rational planning, and multifactor experimental design. Some of these methods require the use of electronic computing machines (ECMs) for data processing, while others can be applied without computational assistance.

Experimental Design: A full factorial experiment (FFE) was utilized to systematically analyze the influence of multiple factors on the properties of foam ceramics. This approach allows for the evaluation of the combined effects of independent variables while minimizing the total number of experiments.

Materials

Local natural and industrial materials were used in the study to produce highly porous foam ceramics with a density of D600–D700. The primary raw materials included clay from the Koskuduk deposit and loam from the Burunday deposit, both characterized by optimal physicochemical and technological properties. To improve the structure and strength, construction gypsum, sodium silicate, and fly ash from thermal power plants were added [36–39]. Foaming was carried out using two types of foaming agents, "PB-2000" and "IFoamOrganic", which ensured the formation of a uniform cellular structure in the foam ceramic samples. To stabilize the structure and regulate coagulation processes, polycarboxylate additives SP-1 and KH-5 were used. The study involved analyzing the physical and mechanical properties of the resulting materials and assessing the effects of various additives on the structural stability and the reduction in shrinkage deformations.

IFoamOrganic is a keratin-based foaming agent derived from animal horns and hooves. It is commonly used in the production of thermal insulation blocks. Compared to synthetic foaming agents, keratin-based foam is known for its higher stability—both during the mixing with mineral components and during the setting phase of the molded ceramic mass.

In this study, both IFoamOrganic and PB-2000 were tested to evaluate their impact on foam structure and material performance.

Physical and Mechanical Properties of IFoamOrganic:

- Working solution concentration: 2.5–3.5%,
- Syneresis time: 10 min,
- Physical state: liquid,
- Density: 1.12–1.15 g/cm^{3,}
- pH at 20 °C: 6.5–7.2,
- Expansion ratio (foamability): ≥6,
- Foam stability: 55 min,
- Shelf life: up to 12 months,
- Color: dark brown,

The PB-2000 foaming agent (TU 2481-185-05744685-01) is a light brown, water-based surfactant solution with a density of 1.0–1.2 g/cm^3 at 20 °C and a pH range of 7.0–10.0.

Preparation Method

Step 1. Preparation of Clay Slip

Raw clay is dispersed in water with the addition of electrolytes such as polysilicates and polycarboxylates. This creates a stable, highly fluid suspension (slip). The electrolytes bind with coagulating cations and release bound water by adsorbing anions onto the clay particle surfaces, improving liquefaction.

Step 2. Introduction of Sodium Silicate (Na_2SiO_3)

Adding sodium silicate promotes the exchange of Ca^{2+} cations in the clay's sorbed complex with monovalent Na^+ ions. This replacement leads to:

- An excess negative surface charge on clay particles, causing repulsion and dispersion into finer grains.
- Released Ca^{2+} cations reacting with silicate anions (SiO_3^{2-}) to form insoluble calcium metasilicate ($CaSiO_3$), further enhancing fluidity.

Step 3. Electrolyte Reaction Mechanism

Adding sodium silicate (Na_2SiO_3) plays a crucial role in modifying the structure of clay during the preparation of the ceramic slip. It promotes the displacement of divalent calcium ions (Ca^{2+}) from the sorption complex of clay minerals, replacing them with monovalent sodium ions (Na^+). This ionic exchange increases the negative surface charge of clay particles, which leads to electrostatic repulsion between them. As a result, aggregated clay particles disintegrate into finer, elementary grains, enhancing the homogeneity and plasticity of the suspension.

Purity and Manufacturer of Sodium Silicate

The sodium silicate used in this study was of industrial grade, with a purity of 98%, and was sourced from Omsk Plant of Industrial and Household Chemistry. This company was established in the 1990s by a group of specialists from aerospace and defense enterprises in Omsk, Russia. The high purity level ensures consistent chemical behavior and reliable performance in the modification of the clay structure during the preparation of the slip.

In aqueous suspension, sodium silicate dissociates into Na^+, Na^+, and SiO_3^{2-} ions. The released Na^+ ions primarily act within the diffusion layer, replacing Ca^{2+} ions that normally bind clay particles into flocs. The freed Ca^{2+} ions then react with silicate anions (SiO_3^{2-}), forming insoluble calcium metasilicate ($CaSiO_3$). This is represented as follows:

$$Ca^{2+} + (SiO_3^{2-}) = CaSiO_3, \quad (2)$$

and this precipitation reaction further contributes to the release of bound water, increasing the amount of free water in the system and enhancing the fluidity and workability of the clay slip.

Step 4. Limiting Electrolyte Concentration

Liquefaction improves only up to a certain electrolyte threshold.

- Excess Na^+ and Ca^{2+} ions form new hydration shells or precipitates.
- Beyond optimal concentrations, free water decreases, suspension viscosity increases, and particles begin to coagulate, reducing fluidity.

Step 5. Role of Electrolytes and Coagulants

Optimized concentrations of electrolytes and coagulants are crucial for:

- Controlling slip fluidity,
- Reducing shrinkage,
- Achieving stable, strong foam ceramic structures.

Step 6. Addition of Fly Ash and Sawdust (Organic Fillers)

For economic and ecological reasons, fly ash is added to reduce clay and fuel consumption:

- It acts as a mineral filler, improving moldability and reducing energy demand,
- The optimal clay-to-ash ratio was determined experimentally (15–50% clay by dry mass).

To reduce shrinkage and enhance drying:

- Sawdust (10–20% by dry mass, ground to 10 μm) is added, improving permeability and reducing drying time,
- Fly ash (10–20% by dry mass) further aids in reducing shrinkage and increasing porosity.

Step 7. Evaluation of Drying Performance

After forming the samples, drying is conducted under controlled conditions.

- Visual inspection (Figure 2) confirms that samples show no visible cracks or shrinkage deformations after drying.



(**a**) (**b**)

Figure 2. Foam ceramic samples before and after drying: (**a**) sample before drying; (**b**) sample after drying.

Step 8. Optimization of Batch Composition and Firing Regime

Once the drying process is optimized, the next stage involves adjusting the raw mix composition and determining the appropriate firing temperature to achieve the desired mechanical and thermal properties in the final foam ceramic products.

Optimization of Foam Ceramics

We have described the technology and composition for preparing foam ceramics. Based on this composition, we will now determine the optimal formulation and plan experiments to assess the following physical and mechanical properties.

Using the developed technology and composition of the foam ceramic mass, component optimization is conducted to achieve superior physical and mechanical properties. Methods of mathematical modeling and experimental design are employed for this purpose. Key parameters for optimization include the clay-to-ash ratio, the concentration of coagulants and electrolytes, as well as the molding and firing conditions.

The experimental planning focuses on determining the physical and mechanical properties of foam ceramic products.

The fired samples undergo the following tests: determination of firing and total shrinkage, bulk density, water absorption, firing quality, and strength limits.

The most important structural and operational properties of foam ceramic products depend on bulk density and true porosity. As demonstrated above, bulk density is determined by the composition of the initial mixture, primarily the surfactant content.

Determination of Air and Firing Shrinkage

Air and firing shrinkage were measured according to GOST 32026–2012 [40], which regulates the procedures for determining the key technological properties of clay raw materials used in expanded ceramic and lightweight aggregate production. This standard provides guidelines for sample preparation, drying, firing, and measurement techniques, ensuring consistency and comparability of results. It is particularly relevant for characterizing shrinkage behavior under thermal treatment in ceramic materials.

The clay raw material was mixed with water to achieve molding moisture and then shaped into samples. After molding, two intersecting diagonal lines were carefully drawn on the tiles using a sharp tool and a ruler. The samples were dried in a SNOL drying oven at 100 °C until a constant mass was achieved. The dried samples were cooled in a desiccator, inspected for defects, and the distance between shrinkage marks was measured with calipers. Air shrinkage was determined by the difference in distances between the marks on molded samples before and after drying.

Firing shrinkage was measured on dried samples. The samples were fired in a laboratory electric muffle furnace (SNOL 6.7/1300). Firing shrinkage was calculated as the difference in distances between the shrinkage marks on the molded, dried, and fired samples.

The raw materials were dried at a temperature of 110 °C and ground until they passed through a 0.63 mm sieve. Then, batch compositions were prepared. The components were mixed in dry form. The prepared batch was moistened to form a slurry with a specified moisture content. Using the casting method, 7 × 7 × 7 cm samples were molded from the slurry.

The samples were then dried at 20 °C for 9.5–10 h, followed by drying at 60 °C in a drying oven until the moisture content reached 1–2%. The dried samples were fired with a holding time of 2 h at a maximum temperature of 1000 °C.

Shrinkage is a critical parameter in foam ceramic production because it directly affects the dimensional stability, mechanical strength, and microstructure of the final product. Excessive shrinkage can lead to cracks, deformation, and poor fit in construction applications, while insufficient shrinkage may indicate incomplete sintering. Accurate control of shrinkage ensures that the material maintains its intended shape, porosity, and performance characteristics after thermal processing.

Total and linear shrinkage were determined based on changes in linear dimensions. Formulas (3) and (4), which are as follows, were used to calculate volumetric changes in the products after firing:

$$V_{total} = (V_1 - V_3)100/V_1, \quad (3)$$

$$V_{total} = (V_2 - V_3)100/V_1, \quad (4)$$

where V_1 is the volume of the product in the freshly molded state (cm^3), V_2 is the volume in the air-dry state (cm^3), and V_3 is the volume after firing (cm^3).

Water Absorption: The water absorption of fired samples characterizes both the porosity and strength of the ceramic body, as well as the sintering process. Water absorption (%) was determined using Formula (5), which is as follows:

$$W = (m_2 - m_1) \times 100/m_1, \quad (5)$$

where m_1 is the mass of the fired sample (g) and m_2 is the mass of the water-saturated sample (g). Water absorption in foam ceramics varies with thermal treatment conditions and mass composition, depending primarily on the bulk density.

Porosity: True porosity was calculated to assess the internal structure of foam ceramics using Formula (6), which is as follows:

$$P_t = (1 - \rho_m/\rho) \times 100, \quad (6)$$

where ρ_m is the bulk density and ρ is the true density.

Open Porosity: Open porosity (%) was derived from water absorption and bulk density using Formula (7), which is as follows:

$$P_a = W \times 100/\rho_m. \quad (7)$$

Closed Porosity: Closed porosity (%) was determined using the following relation (8), which is as follows:

$$P_x = P_t - P_a. \quad (8)$$

The presence of both open and closed porosity plays a crucial role in balancing the mechanical strength and thermal insulation properties of foam ceramics. Open porosity allows for the material to trap air within its structure, significantly improving thermal insulation by reducing heat transfer. However, excessive open porosity can weaken the mechanical strength, making the material more susceptible to deformation under stress. On the other hand, closed porosity, which is not interconnected, contributes to structural integrity by enhancing the material's ability to resist external forces and improving its overall mechanical strength. A balance between open and closed porosity ensures that foam ceramics achieve optimal thermal insulation without compromising mechanical stability.

Thermal Conductivity: The thermal conductivity of porous ceramic samples was measured using an ITP-MG4 electronic thermal conductivity meter. Both the steady-state heat flux density method and the thermal probe method were applied.

The thermal conductivity of porous ceramic samples was determined experimentally using an electronic thermal conductivity meter of the ITP-MG4 type, employing the steady-state heat flow density method and the thermal probe method applied directly to the samples.

Mechanical Strength: Compressive and flexural strength were tested following GOST 7025-78. Foam ceramic cubes were dried to a residual moisture content of 5–6% and fired at optimal temperatures. Tests were conducted on the PGM-100MG4A press, applying a uniform load at 0.5 MPa/s until failure. The maximum load was recorded for each sample.

The experimental results will support the development of mathematical models to predict the behavior of foam ceramics under varying compositions and processing conditions. This will optimize production, enhancing strength while minimizing energy consumption.

3. Results

The strength of foam ceramic products must meet standards for thermal insulation materials. Based on experiments, the required compressive strength was determined to exceed 1 MPa. Density correlates with thermal conductivity, influencing insulation properties. Products with a density below 0.8–1 g/cm^3 show significant insulation performance, while thermal conductivity rises from 0.6 to 1.7 W/(m·°C) between 20 and 1500 °C.

The goal was to develop foam ceramics based on thermal power plant fly ash, ensuring high strength with minimal density and thermal conductivity for optimal insulation. Comparative properties like water absorption and porosity were also evaluated.

We used computer modeling with the STATSOFT program for statistical experimental planning. A full factorial experimental design was applied, enabling a comprehensive assessment of the influence of each variable and their interactions on the properties of the foam ceramic material. This approach allowed for the development of a second-order regression model based on the results of a complete set of combinations of factor levels, including three parallel trials to assess reproducibility, regression coefficients, and model adequacy.

Objective: To optimize the batch composition and firing temperature for foam ceramics using mathematical modeling and experimental design.

Tasks:

- Encode variables.
- Construct a Box–Behnken planning matrix considering paired interactions.
- Calculate regression coefficients and test their significance.
- Optimize batch composition and firing temperature.
- Build a three-factor experimental matrix.
- Analyze results, verify model adequacy, and assess coefficient significance.
- Optimize process parameters and develop a general model linking responses (y) to factors (x1, x2, x3), identifying minima using classical optimization methods.

A full factorial three-factor experiment (2^3 orthogonal design) was conducted to study physical–mechanical properties. Key optimization parameters included the physical–mechanical properties of the foam ceramics.

Input Variables:

- x1, x2: Loam and fly ash dosage (%).
- x3: Firing temperature (°C).

Loam and fly ash stabilized the porous structure. Loam was chosen for its alkali oxides (Na_2O, K_2O at 15–16%), promoting early melt formation and sintering. Fly ash improved swelling stability and sintering due to its fine dispersion and unburned carbon content, ensuring uniform firing.

Hydraulic ash from the Almaty Combined Heat and Power Plant (CHP) was used in this study. The plant operates an ash and slag disposal site with a total area of 1300 hectares. The properties of the ash were investigated in accordance with the requirements of GOST 25818–2018.

Based on the type of coal used, the ash belongs to the bituminous coal group (KU), which is formed from the combustion of bituminous coal, excluding lean coal.

According to its chemical composition, the ash is classified as acidic, containing up to 10% CaO by mass. Table 1 presents the chemical composition of the ash.

Table 1. Encoding and variation in input factors.

Factor	Code	Levels of Varying Factors			Variation Interval (Δx_i)	Unit
		−1	0	+1		
Loam	x_1	45	55	65	5.0	%
Fly Ash	x_2	10	15	30	5.0	%
Firing Temperature	x_3	850	925	1000	10.0	°C

The ash consists of black and dark gray particles ranging in size from 10 to 100 microns, has a dense glassy structure, and shows low loss on ignition.

The ash was used as a siliceous component in the experiments. The hydraulic ash from the CHP was characterized by the following properties:

- Specific surface area: 2700–2900 cm^2/g.
- Bulk density: 800 kg/m^3.
- True density: 2.65 g/cm^3.
- Loss on ignition: 4.3%.
- Moisture content: 17%.
- Ash activity: 43.8.

A protein-based foaming agent (0.5–1% of dry mass) was used. The water-to-solid ratio ranged from 0.5 to 0.7.

Response Criteria (y): These are physicalmechanical properties like strength, density, thermal conductivity, water absorption, and porosity. Planning conditions, adjustable factors, levels, and variation intervals are shown in Table 1.

The most convenient tool for gradient estimation is the well-developed and tested method of factorial experiments. A series of experiments can be conducted, where all factors take values within a specified range, and the corresponding value of the function y, known as the target parameter, is determined experimentally. Table 2 presents the results of the experimental study.

The planning matrix was constructed using the Box–Behnken method.

The practical value lies in selecting the composition of the initial mixture that ensures the final product has minimal values for indicators y2 and y5, and maximal values for indicators y1, y3, and y4.

The mathematical foundation of experimental design theory is regression analysis, which aims to establish relationships between the target parameter y and the influencing factors of the studied object $x_1, x_2, \ldots, x_j, \ldots, x_k$. Typically, the exact analytical expression of the function $y = f(x_1, x_2, \ldots, x_j, \ldots, x_k)$ remains unknown, requiring its approximation using a polynomial representation (Equation (9)), which is as follows:

$$y = b_0 + b_1 \cdot x_1 + b_2 \cdot x_2 + b_3 \cdot x_3 + b_{12} \cdot x_1 \cdot x_2 + b_{13} \cdot x_1 \cdot x_3 + b_{23} \cdot x_2 \cdot x_3 + b_{123} \cdot x_1 \cdot x_2 \cdot x_3 \quad (9)$$

where b_i, b_j, b_{ij} are the regression coefficients, and x_i, x_j, x_i are the input factors.

The values of the regression coefficients b_i and b_{ij} allow for an assessment of the influence of individual factors and their interactions on the optimization parameter. The greater the numerical value of a coefficient, the stronger the factor's influence. A positive coefficient indicates that an increase in the factor value leads to an increase in the optimization parameter, whereas a negative coefficient signifies a decrease.

Table 2. Planning matrix and experimental results in the study.

#	Input Parameters				Interactions				Optimization Criteria (y = f(x_1, x_2, x_3))					
									y_1 Strength (MPa)		y_2 Thermal Conductivity		y_5 Density (g/cm^3)	
	x_0	x_1	x_2	x_3	x_2x_1	x_2x_3	x_1x_3	$x_1x_2x_3$	Calc.	Avg.	Calc.	Exp.	Calc.	Exp.
1	+	−	−	0	+	0	0	0	1933 1869 1941	1.92	0.149 0.148 0.151	0.15	820 817 819	818,666
2	+	−	+	0	−	0	0	0	2954 2965 3005	2.98	0.152 0.160 0.157	0.156	830 828 827	828,333
3	+	+	−	0	−	0	0	0	2599 2621 2698	6.45	0.135 0.129 0.130	0.131	790 785 787	787,333
4	+	+	+	0	+	0	0	0	4463 4473 4451	4.45	0.141 0.139 0.137	0.139	750 749 747	748,666
5	+	−	0	−	0	0	+	0	3571 3668 3541	3.59	0.138 0.135 0.137	0.136	754 750 753	752,333
6	+	−	0	+	0	0	−	0	2424 2519 2462	2.47	0.139 0.136 0.134	0.136	770 768 767	768,333
7	+	+	0	−	0	0	−	0	3694 3714 3721	3.72	0.140 0.136 0.139	0.138	790 789 786	788,333
8	+	+	0	+	0	0	+	0	3412 3484 3429	3.44	0.132 0.130 0.126	0.129	687 685 683	685

The regression coefficients are determined using Formula (10), which is as follows:

$$b_j = \frac{\sum_1^N y}{N}; b_j = \frac{\sum_{i=1}^N x_{ij} \cdot y_i}{N} \quad (10)$$

where N = 15 is the number of experiments, and x_i, x_j, x_i are the input factors.

Following the execution of the experiment and data processing using the least squares method (LSM) through the LSM software version 1, the regression coefficients of the experimental statistical models describing the properties of the foam ceramic samples were calculated. For clarity, a table is constructed to summarize the obtained regression equation coefficients (Table 3).

Table 3. Regression coefficients results.

No	b_0	b_1	b_2	b_3	b_{12}	b_{13}	b_{23}	b_{123}
y_1	3.310	0.36	0.47	0.45	0.2	−0.08	0.16	0.91
y_2	0.146	0.004	0.012	0.028	−0.001	0.003	0.002	0.044
y_3	68.66	3.555	6.34	13.23	0.71	−1.336	−6.81	19.61
y_4	53.22	2.447	5.07	10.54	−0.52	−0.331	−0.323	15.21
y_5	722.2	29.61	77.47	145.5	−11.92	15.42	−4.52	233.02

We formulate the regression equations with respect to the new variables:

Compressive strength (11) is as follows:

$$y_1 = 3.31 + 0.36x_1 + 0.47x_2 + 0.45x_3 + 0.21x_1x_2 - 0.08x_1\,x_3 + 0.16x_2x_3 + 0.91x_1x_2x_3 \quad (11)$$

Thermal conductivity (12) is as follows:

$$y_2 = 0.146 + 0.004x_1 + 0.012x_2 + 0.028x_3 - 0.001x_1\,x_2 + 0.003x_1\,x_3 + 0.002x_2\,x_3 + 0.044x_1\,x_2\,x_3 \quad (12)$$

Porosity (13) is as follows:

$$y_3 = 68.66 + 3.555x_1 + 6.34x_2 + 13.23x_3 + 0.71x_1\,x_2 - 1.336x_1\,x_3 - 6.81x_2\,x_3 + 19.61x_1\,x_2\,x_3 \quad (13)$$

Water absorption (14) is as follows:

$$y_4 = 53.22 + 2.447x_1 + 5.07x_2 + 10.54x_3 - 0.52x_1\,x_2 - 0.331x_1\,x_3 - 0.323x_2\,x_3 + 15.21x_1\,x_3 \quad (14)$$

Density (15) is as follows:

$$y_5 = 722.2 + 29.61x_1 + 77.47x_2 + 145.5x_3 - 11.92x_1\,x_2 + 15.42x_1\,x_3 - 4.52x_2\,x_3 + 223.02x_1\,x_2\,x_3 \quad (15)$$

After obtaining the mathematical model, the significance of the regression coefficients (i.e., their deviation from zero) and the adequacy of the model are evaluated. The significance of the coefficients is tested using Student's *t*-test, which is calculated using Equation (16).

For foam ceramics, a threshold p value of 0.05 was used to determine the statistical significance of the regression coefficients. Coefficients with p values below this threshold were considered to have a significant influence on the response variables such as compressive strength, porosity, and thermal conductivity. This ensured that only the most relevant factors were included in the final model. Equation (16) is as follows:

$$t_i = \frac{|b_i|}{S\{b_i\}} \quad (16)$$

where b_i is the i-th regression coefficient, and $S\{b_i\}$ is the standard deviation in the determination of the coefficients.

The standard deviation is determined based on the variance of the reproducibility of results across all conducted experiments and is calculated using Equation (17), which is as follows:

$$S_i^2 = \frac{\sum_1^n (y_i - y^-)^2}{n-1} \quad (17)$$

where y is the arithmetic mean value of the optimization parameter obtained from five repeated experiments.

After determining the reproducibility variance, a table is constructed for clarity and convenience to present the response values (y_1, y_3, y_4) (Table 1).

The degrees of freedom are calculated using Equation (18), which is as follows:

$$f_1 = N(n-1) = 20\cdot(3-1) = 40. \quad (18)$$

Since the value of Student's *t*-test for the number of observations $f_1 = 40$ and a 95% confidence level is 2.021 (according to the reference table), the comparison results for the five optimization criteria are presented in Table 2.

The adequacy of the obtained regression equation with the significant coefficients is verified using Fisher's criterion: if $F_{calc} < F_{tab}$ the equations are considered adequate.

The calculated Fisher's value is determined using Equation (19), which is as follows:

$$F_{\text{calc}} = \frac{S^2_{\text{oct}}}{S^2_{\{y\}}} \tag{19}$$

After verifying the significance of the obtained coefficients and eliminating insignificant ones, the regression equation describing the physical and mechanical properties of foam ceramics as a function of the loam dosage (x_1), fly ash content (x_2), and firing temperature (x_3) is established.

Next, calculations are performed separately for each response variable, and the adequacy of each model is evaluated. Additionally, a quality assessment of each model must be conducted.

Table 4 summarizes the results of the calculations for the analysis.

Table 4. Results of the performed calculations.

No	$S^2_{y_1}$	$S^2_{y_2}$	$S^2_{y_3}$	$S^2_{y_4}$	$S^2_{y_5}$
1	0.0016055	0.000003	0.0007	0.37	2.333334
2	0.000763	0.0000165	0.0006335	0.043334	2.3333335
3	21.784473	0.0000105	0.0002335	0.063334	6.3333335
4	0.0003495	0.000004	0.0001	0.7633335	2.333334
5	0.2873745	0.000003	0.0002335	0.2533335	4.3333335
6	2.448058	0.1375045	64.877178	57.3304445	770.5559445
7	0.0003565	0.0000045	0.28	0.1733335	4.3333335
8	0.0014205	0.0000095	0.01	0.28	4
9	0.001972	0.000009	0.0004335	0.25	4
10	0.010852	0.00001	0.0002335	0.28	154.333334
11	0.0171345	0.0000025	0.01	0.2633335	4.3333335
12	0.002623	0.000007	0.012134	0.253334	2.333334
13	0.0025335	0.0000045	0.010134	0.023334	4.333334
14	0.003823	0.000003	0.0004335	0.163334	6.333334
15	0.0000375	0.0000025	0.004134	0.2533335	4.3333335
16	0.0002645	0.000003	1.013334	0.10315	1.666667
17	0.000066	0.0000045	0.0028	0.182934	3.3884445
18	0.000129	0.0000025	0.0433335	0.002324	6.111889
19	0.0003575	0.000004	0.043334	0.025644	6.8323335
20	0.0003665	0.000003	1.083334	0.37	2.333334
Total:					
$\sum$	24.56456	0.137611	67.39272	61.44783	996.8886
$S^2(y^-)$	0.409409	0.002294	1.123212	1.024131	16.61481
σ	0.639851	0.047896	1.059817	1.011994	4.076127
f_1	1.293139	0.096798	2.14189	2.04524	8.237853
SBOCпр	0.909624	0.06809	1.506656	1.438669	5.794699
F	0.450086	0.033684	0.7455	0.71186	2.867243

The significance of the coefficients is analyzed separately for each response variable.

As a result of mathematical modeling using the obtained equation and the identified model parameters, response graphs were generated to illustrate the dependence of response variables on factor values.

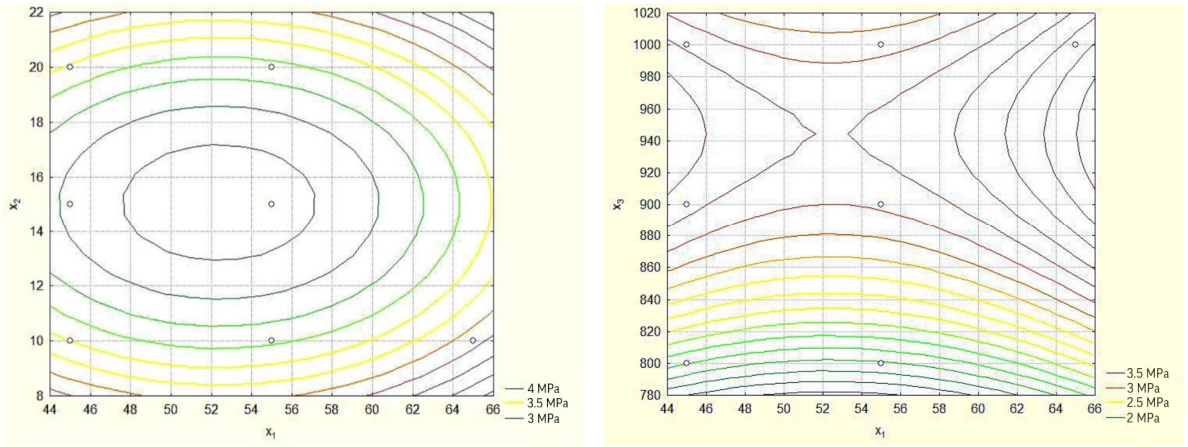
Based on the averaged values, graphical dependencies were constructed to show variations in response parameters (strength, density, thermal conductivity, porosity, and water absorption) as a function of each individual factor, while maintaining the averaged values of the remaining factors.

From a practical perspective, the most valuable composition of the initial mixture is the one that results in the lowest values for y_2 and y_5, while maximizing y_1, y_3, and y_4.

A strength of this is that Student's *t*-test confirmed that the obtained coefficients are statistically significant.

The Fisher criterion test demonstrated that the regression equation is adequate, as the calculated value is lower than the critical threshold ($F < F_{critical}$).

Figure 3 presents the strength variation graphs as a function of the slip composition. The obtained determination coefficient of $R^2 = 0.887$, which is sufficiently close to 1, further confirms the adequacy of the developed mathematical model.



(**a**) (**b**)

Figure 3. Isoline diagram of the mathematical model for foam ceramic strength: (**a**) x_3 = const; (**b**) x_1 = const.

The most significant factors contributing to increased strength are the loam content in the batch and the firing temperature. The fly ash content is the most critical factor influencing the strength of the samples. Fly ash reduces shrinkage in the porous mass, while the development of structural strength occurs more intensively. According to the response graph, this threshold is in the range of 15–20%.

The lowest strength values (1.5–2 MPa) are observed in compositions containing 45–50% loam and 10% fly ash, whereas the highest strength values (4–5 MPa) are achieved in compositions with 55% loam and 15% fly ash. The weakest results are obtained at a firing temperature of 800 °C, while the best results are achieved at 950–1000 °C.

For a visual representation of the samples, refer to Figure 4. The cross-sections of the response surface are shown as vertical lines. In the analysis of foam ceramic strength, the samples were visually categorized based on their compressive strength refer to Figure 5.

Thermal Conductivity: Student's *t*-test confirmed that the obtained coefficients are statistically significant.

The Fisher criterion test demonstrated that the regression equation is adequate, as the calculated value is lower than the critical threshold (F < F_critical).

An increase in firing temperature leads to a rise in thermal conductivity due to densification of the ceramic matrix and a corresponding decrease in total porosity. As the firing temperature increases, pore walls thicken and closed porosity may be partially eliminated, allowing better heat transfer through the solid phase. This effect has been observed in similar studies on foam ceramics, where thermal conductivity increased from 0.09 to 0.15 W/(m·K) as firing temperature rose from 900 °C to 1100 °C. These results are consistent with the trends observed in our regression model.

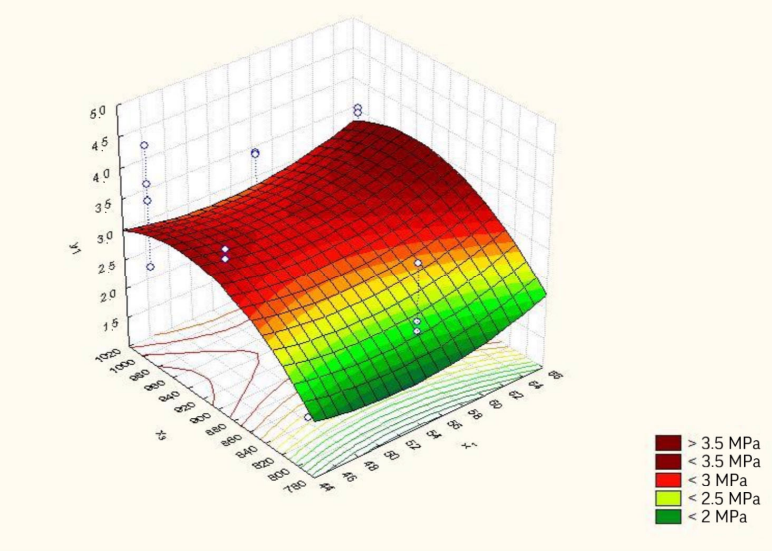


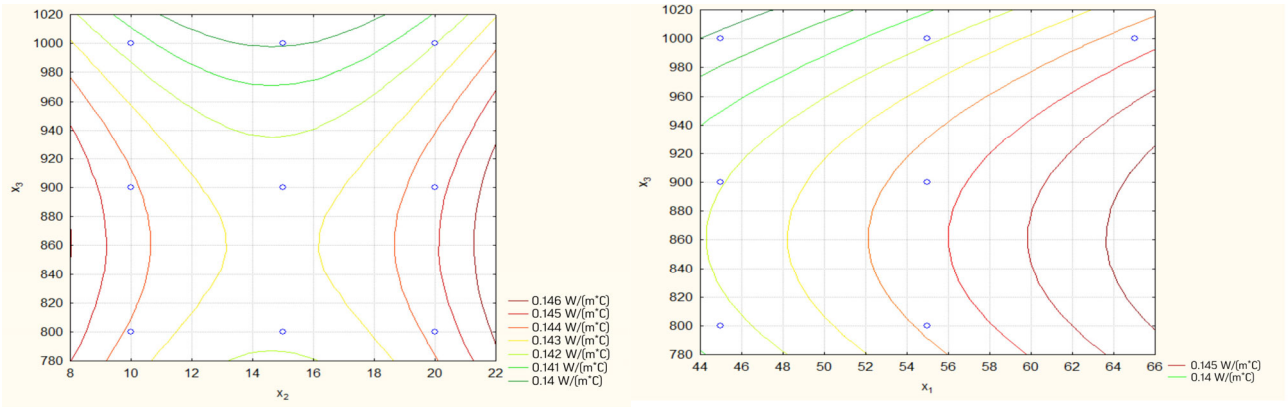
Figure 4. Response surface of y_1 at x_2 = const.



(**a**) (**b**) (**c**)

Figure 5. Visual representation of samples with varying strength: (**a**) 1–1.5 MPa; (**b**) 2.5–3 MPa; (**c**) 3.5–4 MPa.

Figures 6 and 7 present the thermal conductivity variation graphs as a function of the slip composition.



(**a**) (**b**)

Figure 6. Isoline diagram of the mathematical model for foam ceramic thermal conductivity: (**a**) x_1 = const; (**b**) x_2 = const.

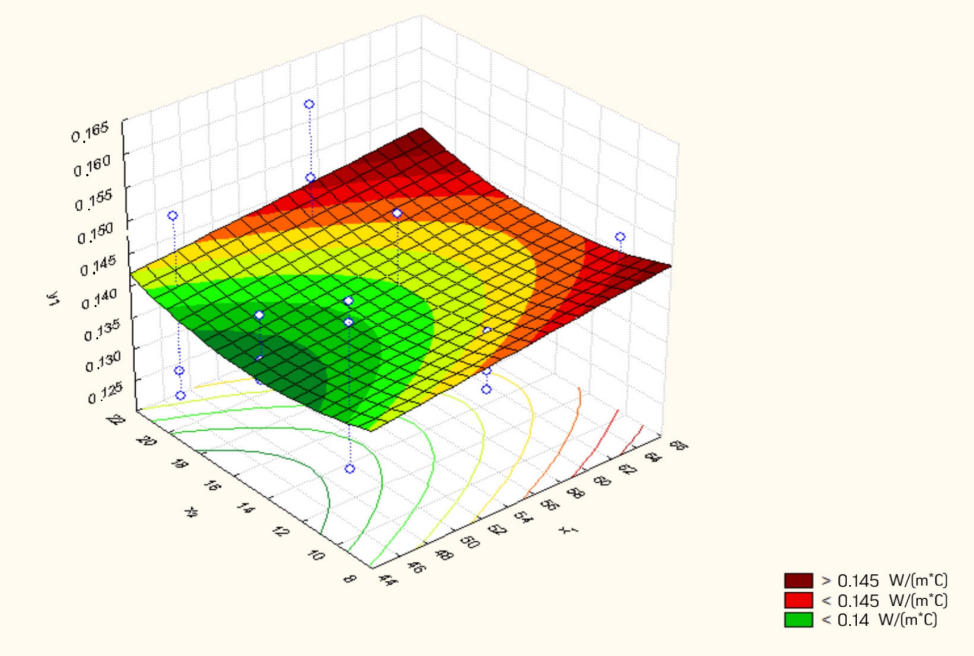


Figure 7. Response surface of y_2 at x_3 = const.

The obtained determination coefficient of R^2 = 0.781, which is sufficiently close to 1, further confirms the adequacy of the developed mathematical model describing the dependence of thermal conductivity on the mixture composition.

The most significant factor reducing thermal conductivity is a fly ash content of 15%, along with a loam content of 45% or 60% and a firing temperature of 950–1000 °C. With an increase in the firing temperature, the thermal conductivity coefficient of the samples also increases.

However, by analyzing parallel dosage compositions, it is possible to determine the optimal fly ash content, ensuring the production of samples with high operational performance.

Porosity: Student's *t*-test confirmed that the obtained coefficients are statistically significant.

The Fisher criterion test demonstrated that the regression equation is adequate, as the calculated value is lower than the critical threshold (F < F_critical).

The obtained determination coefficient of R^2 = 0.882, which is sufficiently close to 1, further confirms the adequacy of the developed mathematical model describing the dependence of porosity on the mixture composition.

The optimal porosity range of 70–72% observed in this study is comparable to or higher than that of many conventional thermal insulation materials, such as lightweight aerated concrete (55–65%) or mineral wool (up to 70%). This high level of porosity contributes to the low thermal conductivity of foam ceramics while maintaining acceptable mechanical strength, making them suitable for energy-efficient construction applications.

Figure 8 presents graphs illustrating the variation in thermal conductivity as a function of mixture composition.

The highest porosity values (70–72%) are observed at 10% fly ash, 55% loam, and a firing temperature of 900 °C. The lowest porosity values (60–65%) are achieved at 15% fly ash, 65% loam, and a firing temperature of 1000 °C.

Figures 8 and 9 illustrate the porosity variation as a function of the slip composition.

For water absorption, Student's *t*-test confirmed that the obtained coefficients are statistically significant.

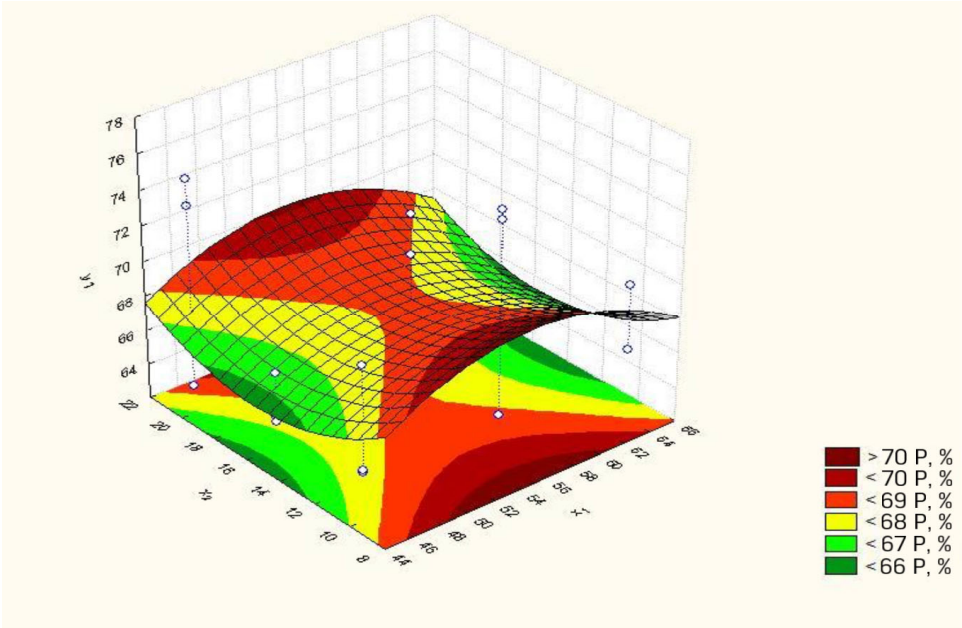
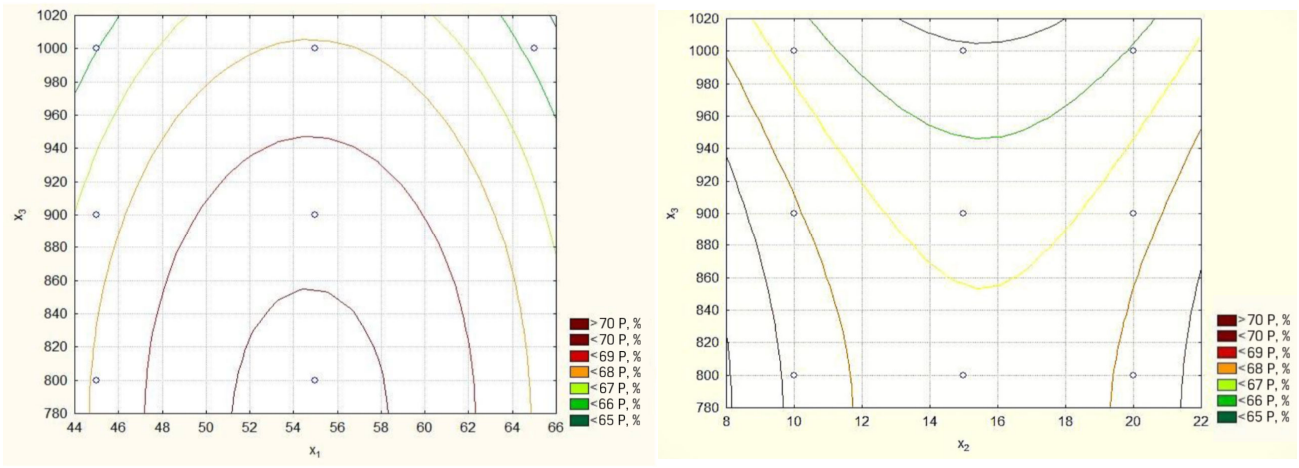


Figure 8. Response surface of y_3 at x_3 = const.



(**a**) (**b**)

Figure 9. Isoline diagram of the mathematical model for foam ceramic porosity: (**a**) x_1 = const; (**b**) x_2 = const.

The Fisher criterion test demonstrated that the regression equation is adequate, as the calculated value is lower than the critical threshold (F < F_critical).

Figures 9 and 10 present the water absorption variation graphs as a function of the slip composition. The cross-sections of the response surface are shown as vertical lines.

The obtained determination coefficient of R^2 = 0.874, which is sufficiently close to 1, further confirms the adequacy of the developed mathematical model describing the dependence of water absorption on the mixture composition and firing temperature.

As the fly ash content in the composition increases, the water absorption of the fired samples also increases. However, it is possible to determine the optimal fly ash dosage, ensuring the production of samples with high operational properties.

The lowest water absorption value (53.1%) is observed in a composition of 10% fly ash, 55% loam, and a firing temperature of 1000 °C.

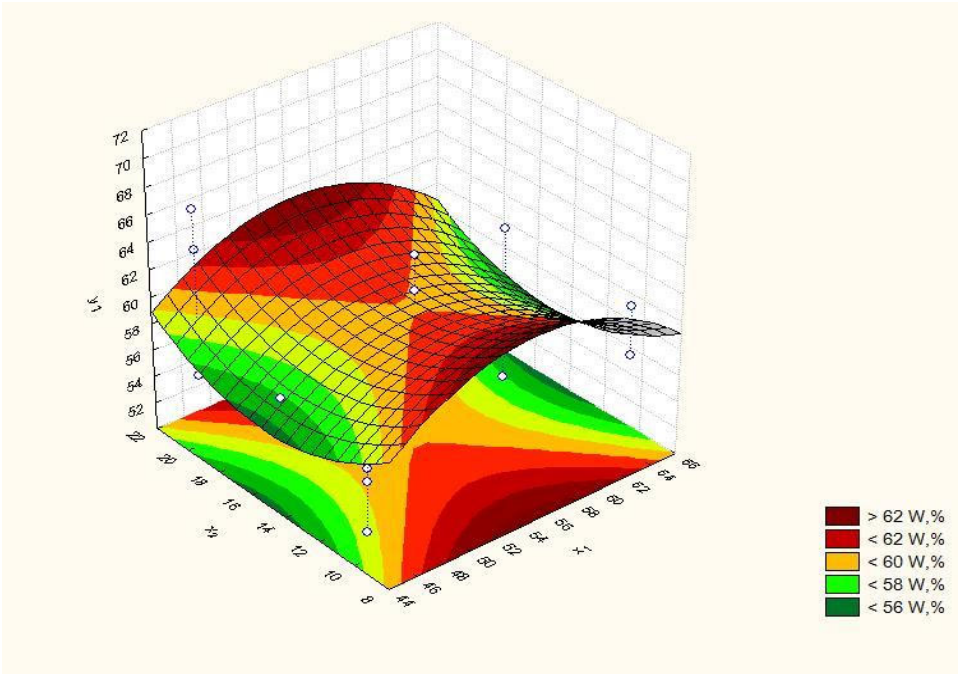
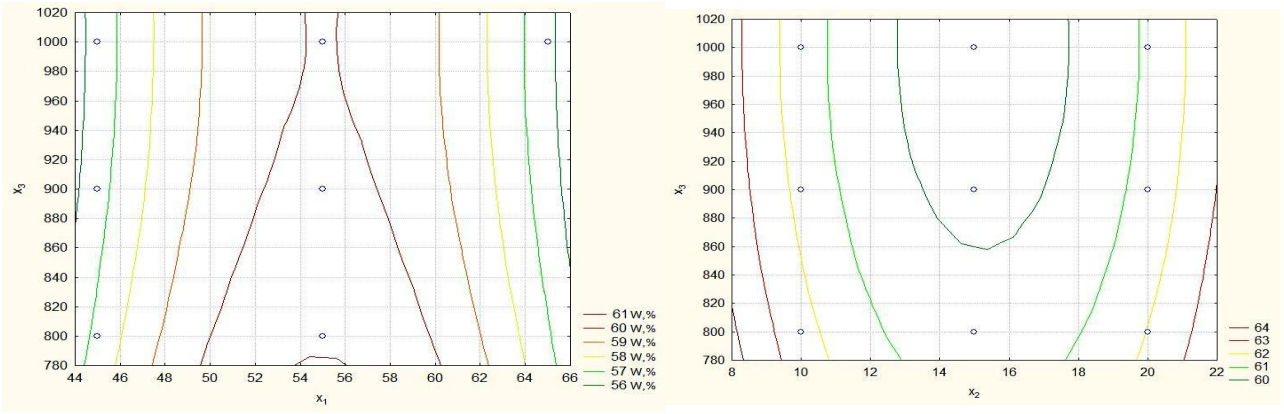


Figure 10. Response surface of y_4 at x_3 = const.

The highest water absorption value (55.6%) is observed in a composition of 20% fly ash, 60% loam, and a firing temperature of 900 °C.

Figure 11 illustrates the isoline diagram of the mathematical model for foam ceramic water absorption at constant values of x_1 and x_2. The cross-sections of the response surface are shown as vertical lines.



(**a**) (**b**)

Figure 11. Isoline diagram of the mathematical model for foam ceramic water absorption: (**a**) x_1 = constx; (**b**) x_2 = const.

Density: Student's *t*-test confirmed that the obtained coefficients are statistically significant.

The Fisher criterion test demonstrated that the regression equation is adequate, as the calculated value is lower than the critical threshold ($F < F_{critical}$).

Figure 12 shows the response surface of the average density y_5 of foam ceramics at constant x_3, illustrating the influence of ash content and firing temperature on density. The cross-sections of the response surface are shown as vertical lines.

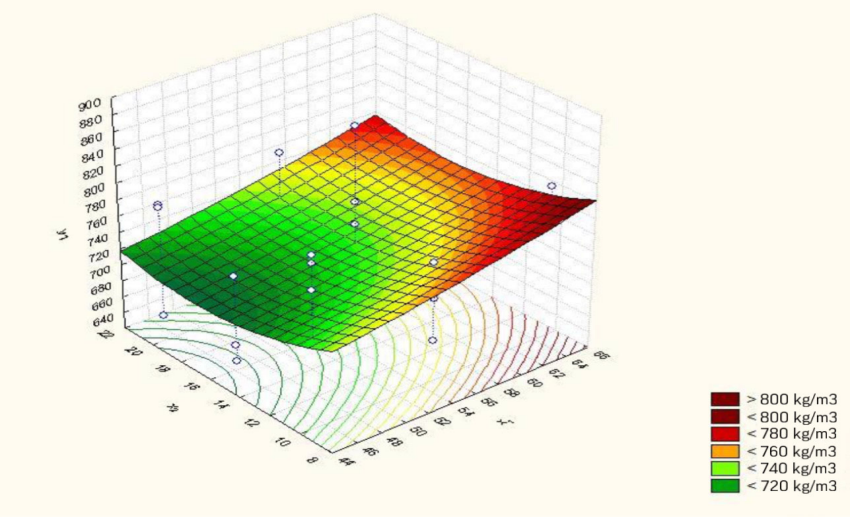
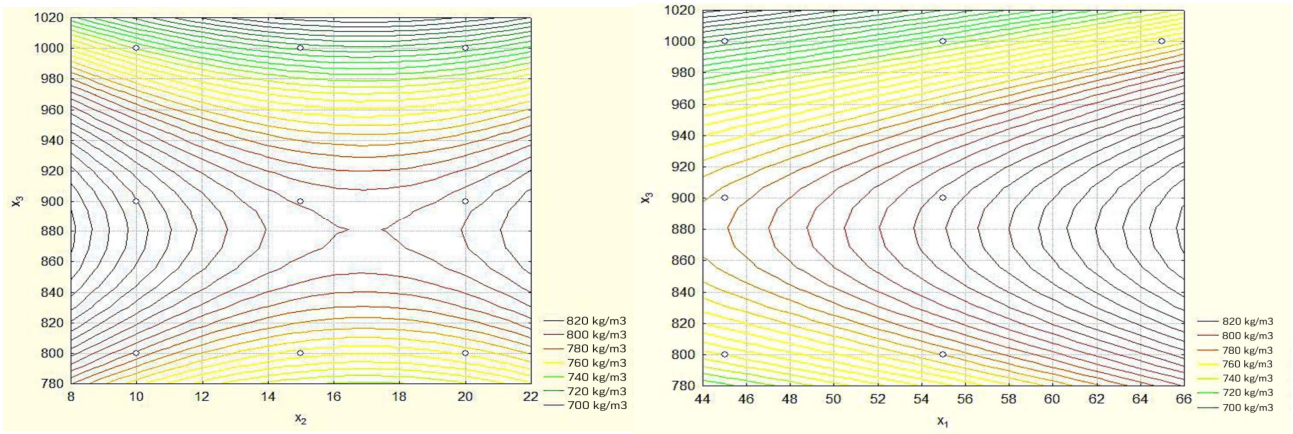


Figure 12. Response surface of y_5 at x_3 = const.

Figures 13 and 14 present the density variation graphs as a function of the slip composition.



(**a**) (**b**)

Figure 13. Isoline diagram of the mathematical model for foam ceramic density: (**a**) x_1 = const; (**b**) x_2 = const.

The optimal average density of foam ceramics (650 kg/m^3) is significantly influenced by the fly ash content in the slip and the firing temperature. Adjusting the slip composition with an optimal fly ash content contributes to reducing the density of the foam ceramic product. However, an excess of fly ash is detrimental as it can negate the positive effects. The optimal fly ash content is 10%.

With an increase in the firing temperature from 900 °C to 1000 °C the average density increases. The optimal firing temperature is considered to be 900 °C as further temperature increases lead to clay melting.

The loam content also affects density; as the loam percentage increases the average density decreases. The optimal loam content is 65%.

A higher average density of 850 kg/m^3 is observed at 20% fly ash, 45% loam, and a firing temperature of 800 °C.

The density range of 650–700 kg/m^3 is considered ideal for foam ceramics because it provides an optimal balance between thermal insulation performance and mechanical strength. In comparison, lightweight aerated concrete has a typical density of 400–700 kg/m^3, while mineral wool ranges from 30 to 200 kg/m^3. Foam ceramics with

densities in this range exhibit lower thermal conductivity than denser materials and yet are mechanically more robust than low-density fibrous insulators. This makes them particularly suitable for structural thermal insulation in energy-efficient buildings.

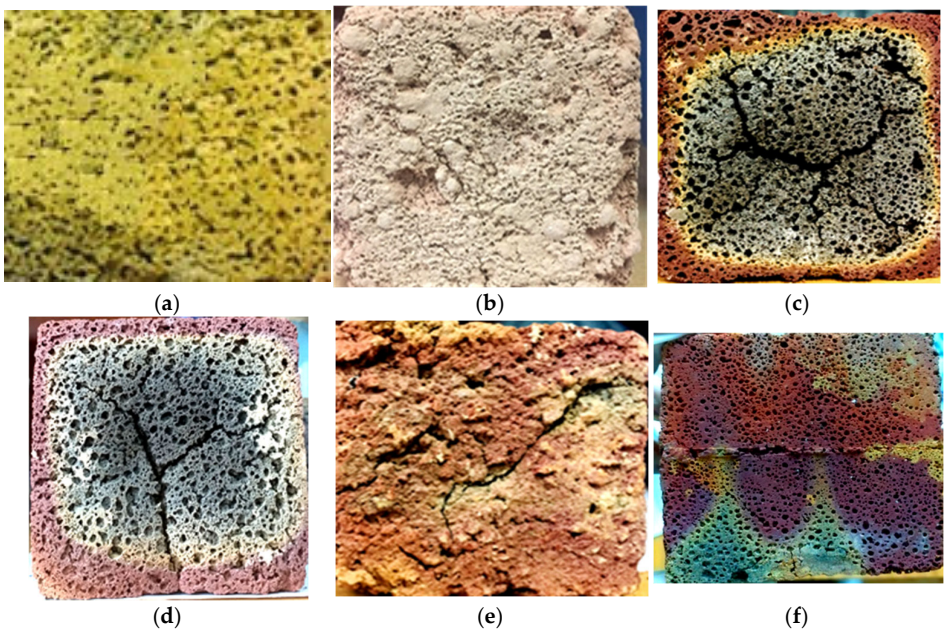


Figure 14. Image of foam ceramic samples with a non-optimal composition (containing gypsum binder). (**a**) Uniform firing without significant defects; (**b**) under-firing; (**c**) uneven firing and over-firing with cracks; (**d**) uneven firing and over-firing with cracks; (**e**) uneven firing with cracks; (**f**) uneven firing.

Optimization of Foam Ceramic Batch Composition

Based on the obtained experimental data and mathematical models, the following conclusions can be drawn. For clarity, a table summarizing the optimal compositions for each response variable is presented (Table 5).

Table 5. Optimal compositions for each response variable.

Optimization Criteria	Loam	Fly Ash	Firing Temperature (°C)	W/S Ratio	Surfactant	Sodium Silicate	Clay	Sawdust
y_1	65	10	1000	0.55	0.5	10	15	10
y_2	55	10	800	0.55	0.5	10	25	10
y_3	55	10	900	0.55	0.5	10	25	10
y_4	60	10	900	0.55	0.5	10	20	10
y_5	55	10	1000	0.55	0.5	10	25	10

It should be noted that foam ceramics with the addition of gypsum binder were completely excluded from consideration. The foam ceramic mass failed to maintain structural integrity, making it impossible to determine the physical and mechanical properties of the samples.

Additionally, samples containing gypsum exhibited uneven firing, further affecting their quality. Visual representations of the foam ceramic samples with a gypsum binder are shown in Figure 15.



(**a**) (**b**) (**c**)

Figure 15. Visual representation of foam ceramic samples with optimal compositions. (**a**) 55% loam; (**b**) 60% loam; (**c**) 65% loam.

Additionally, the use of gypsum is currently environmentally unacceptable as it leads to intensive air pollution with sulfurous gases.

For each sample, the same amounts of water, surfactant, sodium silicate, and sawdust were selected. The table also summarizes the results for each composition.

From the table, it can be observed that the optimal fly ash content for all responses is 10%, and the optimal firing temperature is 900 °C. However, for a more precise selection, the response values must be further analyzed.

Table 6 presents the experimental results for foam ceramic samples with varying loam content and firing temperature, showing their corresponding compressive strength, thermal conductivity, porosity, water absorption, and density.

Table 6. Response values of the optimal composition.

Loam/Firing Temperature	y_1, MPa	y_2, W/(m·°C)	y_3, % Porosity	y_4, % Water Absorption	y_5, kg/m^3
55/1000	3	0.14	60	60	700
60/1000	3.5	0.143	70	65	740
65/1000	4	0.145	69	56	720

Based on the given data, it can be concluded that the optimal composition of foam ceramics is as follows: loam 60–65%, fly ash 10%, clay 15–20%, and a firing temperature of 950–1000 °C.

A visual representation of foam ceramic samples with optimal compositions is shown in Figure 14.

Investigation of the properties of fired foam ceramic products. Fired samples underwent the following tests: determination of fire and total shrinkage, bulk density, water absorption, firing quality, and strength limits.

The most important structural and operational properties of foam ceramic products depend on their bulk density and true porosity. Bulk density is primarily determined by the composition of the initial mixture, particularly the surfactant content.

Total and Fire Shrinkage: The total and linear shrinkage were determined based on changes in linear dimensions.

Table 7 summarizes the results obtained for the total and linear shrinkage of the samples.

Table 7. Shrinkage properties of foam ceramics.

No.	Air Shrinkage, %	Fire Shrinkage, %	Total Shrinkage, %	Volumetric Air Shrinkage, %	Volumetric Fire Shrinkage, %
1	9.6	1.7	10.7	20.5	14.2
2	11.8	2.4	10.9	21.2	15.1
3	10.7	1.5	9.3	20.32	14.1
4	14.1	2	10.5	20.1	13.2

Water Absorption: The water absorption of fired samples serves as an independent characteristic of the ceramic body, defining its porosity, strength, and the sintering process of the material.

The water absorption of foam ceramic products, under slight variations in thermal treatment regimes and mixture composition, primarily depends on their bulk density.

Figure 16 illustrates the influence of the bulk density of foam ceramic products on the W_m and W_y parameters.

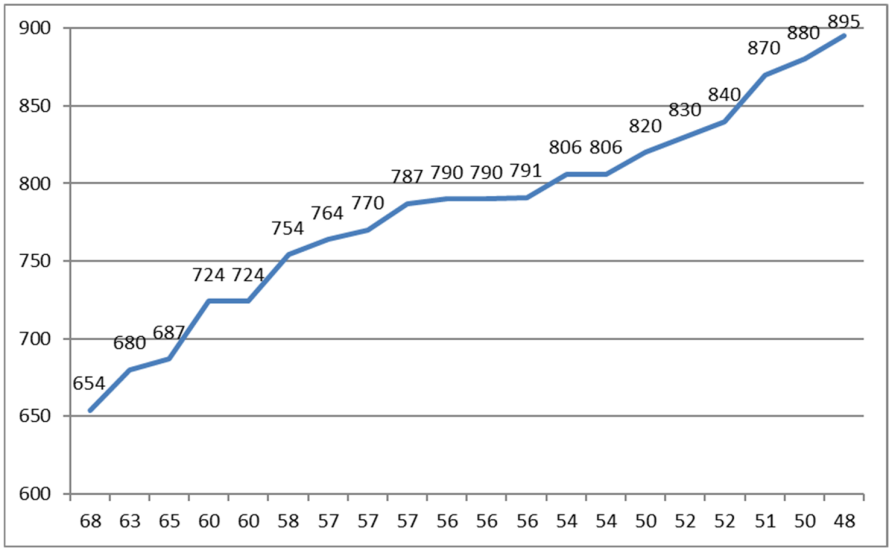


Figure 16. Water absorption of foam ceramic products as a function of bulk density.

Porosity

For foam ceramics, true density has an auxiliary role and is used in the calculation of material porosity.

Based on experimental data, Table 8 summarizes the porosity values.

Table 8. Porosity values of foam ceramic products.

No.	Total Porosity (P_i), %	Open Porosity (P_o), %	Closed Porosity (P_x), %
1	60	8.1	51.9
2	70	9.02	60.9
3	69	9.58	59.4

Mechanical strength is one of the key technical characteristics of ceramic materials. High strength enables their use in load-bearing structures, reduces wall thickness, and allows for increased building height.

The compressive strength of foam ceramic materials, under otherwise equal conditions, depends on their bulk density. Figure 17 presents the results of compressive strength tests

on foam ceramic products. The horizontal axis represents the compressive strength, while the vertical axis shows the density.

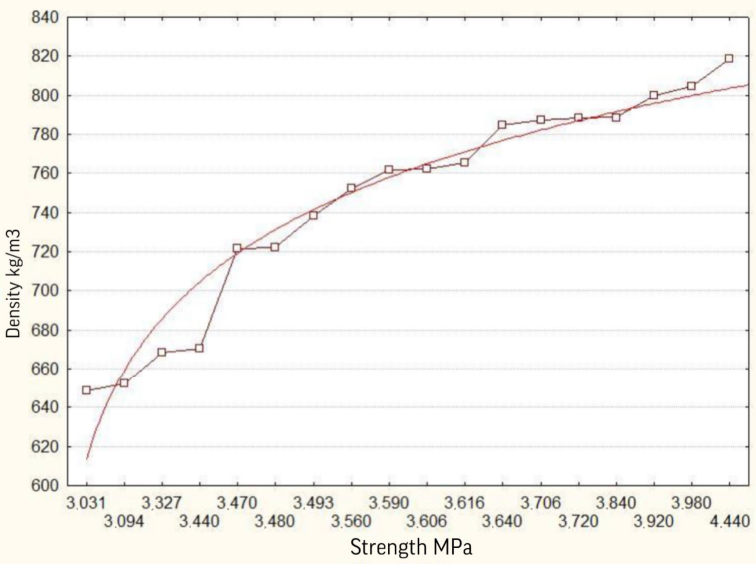


Figure 17. Compressive strength limit of foam ceramic products as a function of bulk density.

The highest strength values were obtained for materials produced from foam ceramic mixtures containing fly ash. However, the addition of more than 10% sawdust to the ceramic mass reduces the strength of the fired products. This effect is less pronounced in certain cases (as indicated by the trend lines in the figure).

Experimental results indicate that the bulk density of foam ceramic products can vary within the range of 800–650 kg/m^3, depending on the raw material composition.

The thermal conductivity of the material depends on bulk density, true porosity, pore size and shape, the type of solid phase, and thermal–moisture influences, among other factors.

Figure 18 presents the relationship between the thermal conductivity of foam ceramic materials and their bulk density.

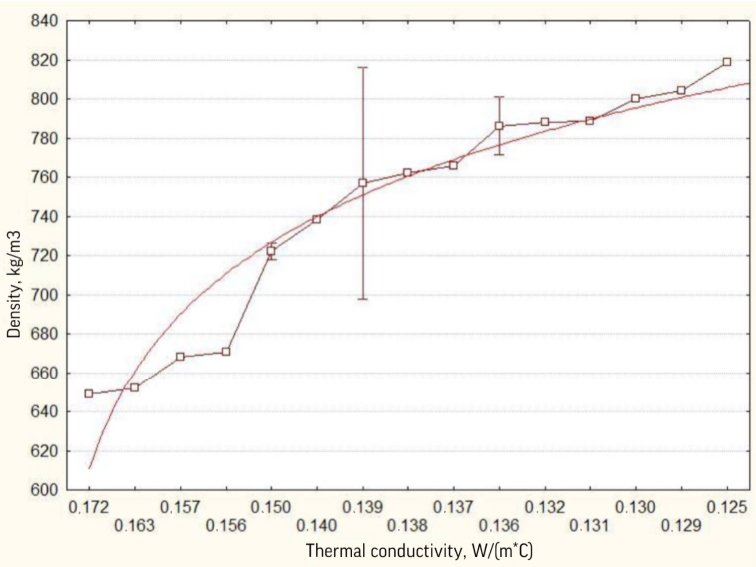


Figure 18. Thermal conductivity of foam ceramic products as a function of bulk density.

Thus, the key properties of fired foam ceramic materials are significantly influenced by the bulk density, porosity, pore size, and pore distribution characteristics.

Following is an investigation and analysis of the phase composition of the optimal foam ceramic sample. As previously described, during the firing process, foam ceramic products undergo various volumetric and linear changes (expansion, shrinkage) as a result of physicochemical transformations. Dilatometric studies allow for determining the sintering onset temperature of foam ceramic materials, analyzing the effect of temperature on dimensional changes, and obtaining essential data for designing and optimizing the firing regime. Figures 19 and 20 present X-ray diffraction patterns of foam ceramic products.

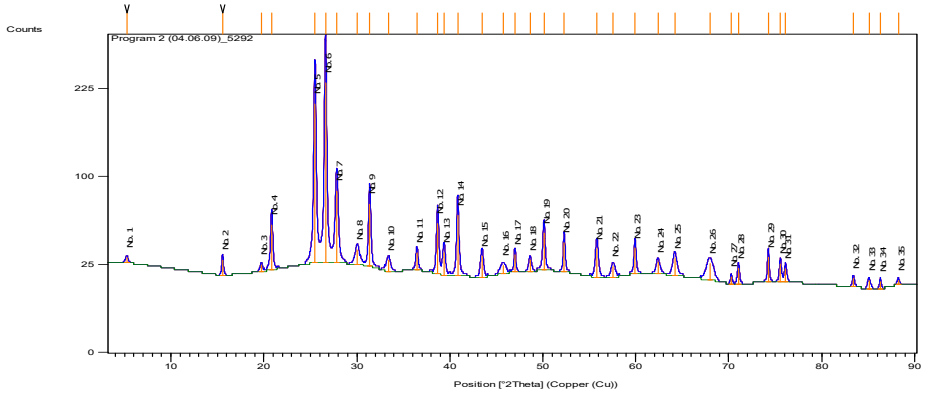


Figure 19. X-ray diffraction patterns of foam ceramic products fired at 900 and 1000 °C, lines from No. 2 to No. 35.

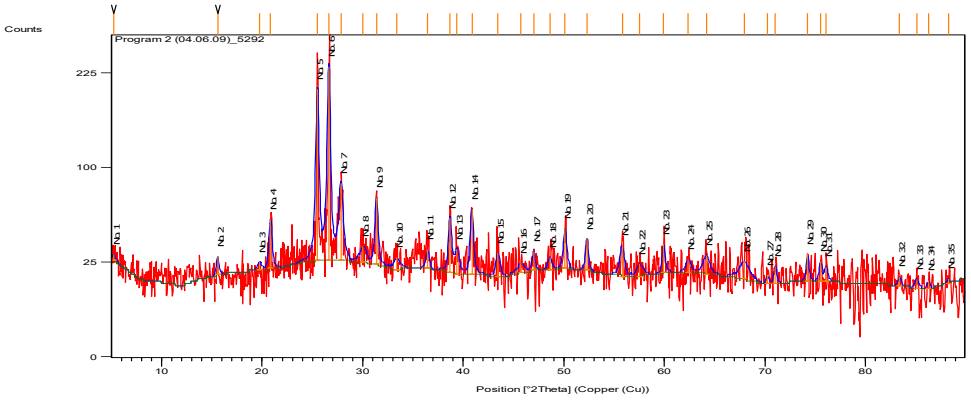


Figure 20. X-ray diffraction patterns of foam ceramic products fired at 950 and 1000 °C.

X-ray phase analysis of the raw material and fired products was performed on a DRON-4 X-ray diffractometer with Cu radiation and a Ni filter, operating at 40 kV and 20 mA using a NaI(Tl) scintillation detector. The interplanar distances were evaluated based on the angle values from the tables of Ya.D. Giller, and the mineral composition was deciphered using the X-ray references from V.I. Mikheev.

The accessories included with the instrument allow for the study of the structure of crystalline and amorphous materials, such as the following:

- Accurate determination of the lattice parameters of crystalline substances;
- Determination of crystallite sizes;
- Study of the material's stress state (first- and second-order stresses);
- Study of textures;
- Qualitative and quantitative phase analysis;
- Investigation of structural changes occurring in deformed metals upon heating.

For the macroscopic characterization of foam ceramic materials, an MBI-1 microscope was used.

X-ray phase analysis confirmed that the phase composition of the synthesized materials is primarily represented by mullite ($3Al_2O_3 \cdot 2SiO_2$), quartz (α-SiO_2), and cristobalite (SiO_2). The effect of firing temperature on the phase composition of optimized samples was examined.

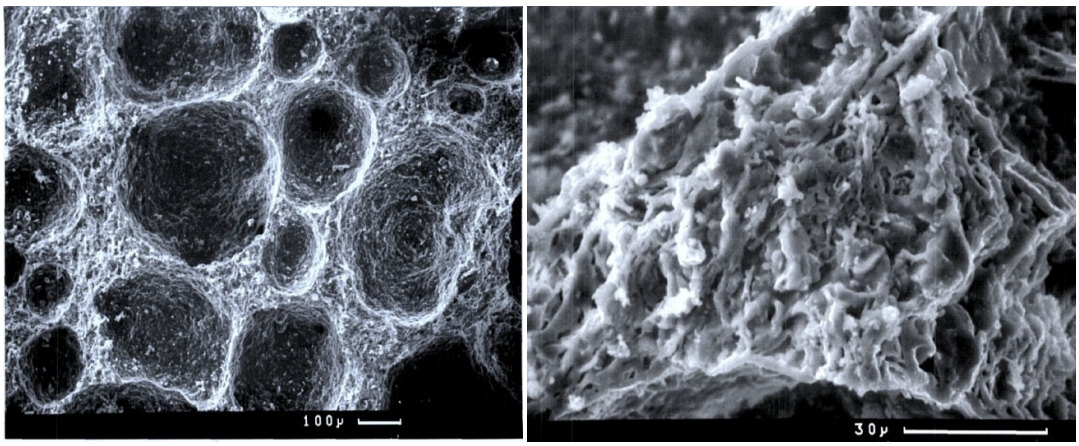
Increasing the firing temperature from 900 °C to 1000 °C leads to a decrease in the intensity of diffraction maxima characteristic of α-quartz, while the intensity of cristobalite diffraction maxima increases, which indirectly suggests changes in their respective quantities.

At the same time, the intensity of peaks corresponding to the crystalline mullite phase remains nearly unchanged. The presence of a mullite crystalline phase in the material structure provides the required strength characteristics.

Phase composition analysis revealed that upon firing foam ceramic masses at 950 °C and 1000 °C, diffraction reflections of clay minerals (lines from No. 2 to No. 35) were absent. This confirms derivatographic analysis data indicating their decomposition.

Furthermore, although cristobalite is known for its high thermal expansion coefficient (CTE), which can lead to reduced thermal shock resistance, its impact in this study was mitigated by the foam ceramics' high porosity. The porous structure absorbs thermal stress and prevents crack propagation during heating and cooling cycles. Thus, despite the presence of cristobalite, the overall thermal performance and structural integrity of the foam ceramics remained acceptable for typical building insulation applications.

As a result of the conducted research, it was established that the macrostructure of foam ceramic products with a bulk density of 650–700 kg/m^3 is characterized by a high number of pores with diameters ranging from 0.2 to 1.5 mm (Figure 21).



(**a**) (**b**)

Figure 21. The macrostructure of foam ceramic products: (**a**) at 100× magnification; (**b**) at 30× magnification.

Notably, the highest pore distribution in these products falls within the 0.2–0.6 mm range, which is significantly different from raw material-based products.

This suggests enhanced structural and operational properties of the foam ceramic materials. Figure 21 presents photographs of the macrostructure of foam ceramic products.

Analysis of the obtained micro-photographs confirmed that the material exhibits significant porosity. The evenly distributed pores throughout the material have an isometric shape and an average size of 750 μm.

The pore size range (0.2–1.5 mm) was measured using optical microscopy with digital image analysis software, version 1. Micrographs were taken using a ZEISS Axio Imager

optical microscope, and pore dimensions were determined by processing the images with calibrated scale bars and averaging across multiple fields of view.

On the fracture surfaces, crystalline formations in the form of elongated prisms were observed. Based on their habit, these crystals can be identified as mullite. Aggregations of crystals of various shapes and sizes are present both on the surface and within the internal pore cavities and are consistent across all tested compositions.

In certain areas, chamotte grains with residual amorphized clay material were also identified.

4. Discussion

The results of this study provide significant insights into the optimization of foam ceramic materials, particularly concerning their mechanical strength, thermal conductivity, porosity, water absorption, and density. The primary objective of this research was to enhance the structural integrity and thermal insulation properties of foam ceramics by optimizing their composition and firing temperature through mathematical modeling and experimental validation.

One of the key findings of this study is the substantial influence of loam and fly ash content on the mechanical strength of foam ceramics. The experiments demonstrated that an optimal composition, consisting of 60–65% loam, 10% fly ash, and a firing temperature of 950–1000 °C, resulted in foam ceramic samples with the highest compressive strength (3.5–4 MPa) and superior thermal insulation properties. This confirms the role of controlled porosity and well-distributed fine pores in enhancing both strength and insulation performance. The optimization of the clay-to-ash ratio plays a critical role in controlling the formation and stability of the porous structure. A balanced clay-to-ash ratio ensures that the material has sufficient binder properties, enhancing the structural integrity of the foam while also maintaining the desired porosity for thermal insulation. Increasing the fly ash content too much leads to higher porosity, which can negatively affect the mechanical properties by weakening the structure.

Additionally, the concentration of coagulants and electrolytes affects the stability and distribution of the pores. Coagulants help regulate the coagulation process, ensuring uniformity in the pore structure, while electrolytes help in dispersing the particles and improving the fluidity of the suspension. The optimized levels of these additives contribute to a stable, well-distributed pore structure that enhances the material's mechanical properties and thermal performance.

Excessive fly ash content was found to negatively impact mechanical properties by increasing porosity beyond optimal levels, leading to reduced structural integrity.

Furthermore, the analysis of thermal conductivity revealed that it is primarily dependent on density and porosity. The obtained regression model (R^2 = 0.781) confirmed the adequacy of the mathematical approach used to predict thermal conductivity. The experimental data showed that increasing the firing temperature from 900 °C to 1000 °C led to an increase in the thermal conductivity due to enhanced densification and reduced air voids. However, an excessive increase in temperature beyond 1000 °C resulted in partial melting of the clay matrix, which could compromise the structural stability of the material.

The study also investigated the impact of porosity on the overall performance of foam ceramics. The experimental results indicated that porosity values between 70 and 72% were optimal for achieving a balance between mechanical strength and thermal insulation. At lower porosity levels (<60%) the density increased significantly, leading to higher thermal conductivity and reduced insulation efficiency. Conversely, at excessively high porosity levels (>75%) mechanical strength deteriorated, making the material less suitable for structural applications.

Water absorption, another critical factor influencing the durability of foam ceramics, was found to be strongly correlated with porosity and bulk density. The regression model (R^2 = 0.874) accurately described the dependence of water absorption on the composition and the firing parameters. The lowest water absorption values (53.1%) were achieved at 10% fly ash, 55% loam, and a firing temperature of 1000 °C. Higher fly ash content increased water absorption due to the formation of interconnected pore networks, which facilitated capillary water uptake.

The density optimization experiments demonstrated that the most suitable compositions yielded foam ceramics with a bulk density of 650–700 kg/m^3, which aligns with the target specifications for lightweight thermal insulation materials. The regression model (R^2 = 0.882) confirmed that the combination of 10% fly ash and 65% loam provided the most favorable balance between density and insulation properties. Increasing the firing temperature from 900 °C to 1000 °C led to higher densification, whereas exceeding this temperature threshold resulted in unwanted vitrification effects.

X-ray diffraction analysis further supported these findings by revealing that the primary crystalline phases in the optimized foam ceramics included mullite, quartz, and cristobalite. The formation of mullite at higher temperatures contributed to improved mechanical properties, while the presence of cristobalite indicated potential trade-offs in the thermal expansion behavior. The phase composition analysis also confirmed that all clay minerals decomposed during firing, ensuring the stability of the final material.

The macroscopic and microscopic structural analysis revealed that the optimized foam ceramics possessed a highly uniform pore distribution, with dominant pore sizes ranging between 0.2 mm and 0.6 mm. This structure contributed to improved thermal insulation performance while maintaining adequate mechanical strength. The microstructural observations also confirmed the presence of mullite crystallites, which reinforced the structural framework of the material.

The percentage of the mullite phase in the final structure is around 20–25%. This proportion is consistent with other ceramic materials used for similar applications, where mullite is typically present at similar levels to enhance strength and thermal stability. In comparison to conventional insulating ceramics, where mullite content may vary, the 20–25% range in foam ceramics provides a balance between mechanical strength and thermal insulation efficiency.

The persistence of the mullite phase across the examined temperature range significantly contributes to the mechanical stability of the foam ceramics, particularly in terms of thermal shock resistance. Mullite's high thermal stability and low thermal expansion coefficient help to mitigate the stresses induced by temperature changes, improving the material's ability to withstand thermal cycling without cracking or degradation. This makes mullite a crucial phase for ensuring the durability of foam ceramics in environments with frequent temperature fluctuations.

Overall, this study demonstrates that mathematical modeling and experimental validation can be effectively combined to optimize the composition and processing conditions of foam ceramics. The findings highlight the potential for producing high-performance, lightweight, and thermally insulating materials suitable for construction and energy-efficient applications. Future research should focus on refining the sintering process, exploring alternative additives for enhanced durability, and investigating the long-term performance of foam ceramics under real-world environmental conditions.

5. Conclusions

The drying and firing processes of foam ceramic materials exhibit several distinct characteristics, influenced by the manufacturing method, the physicochemical and tech-

nological properties of clay raw materials and additives, and the nature of the porous structure. The coagulation ability of clay raw materials enhances the structural strength of the green body in the initial drying stage, allowing for demolding within 2–3 h after forming, which accelerates the drying process. The introduction of 10% sawdust reduces air shrinkage, improving the dimensional stability of the material.

Through mathematical modeling, an optimized method for producing ceramic products was developed with the following composition: loam (60–65%), fly ash (10%), and clay (15–20%), fired at 950–1000 °C. The resulting material has a bulk density of 680–700 kg/m^3, a compressive strength of 3.5–4 MPa, and a thermal conductivity of 0.135–0.140 W/(m·K). The high-porosity structure of foam ceramics allows for the intensification of the firing process, leading to energy savings and improved efficiency.

Achieving high-strength foam ceramic materials is possible by creating a fine-pore structure with densely packed pore walls, which minimizes the formation of cracks and defects. The coagulation ability of clay raw materials plays a crucial role in determining the physical and technical properties of the final product, particularly its bulk density, porosity, pore size, and pore distribution.

The optimization of drying and firing conditions using mathematical modeling and predictive analysis has identified the optimal drying time as 9.5 h at a temperature of 90 °C. This drying time is relatively shorter than conventional drying times for similar materials, which typically range from 12 to 24 h, depending on the material and environmental conditions. The optimized drying process significantly improves energy efficiency and production time, contributing to the overall performance of foam ceramics. These optimized parameters contribute to improving the structural integrity and performance of foam ceramic products.

Author Contributions: Conceptualization, A.K. and S.N.; methodology, I.T.; software, R.S.; validation, N.A., L.M. and A.N.; formal analysis, I.R.; investigation, A.Y.; resources, A.K.; data curation, S.N.; writing—original draft preparation, I.T.; writing—review and editing, R.S. All authors have read and agreed to the published version of the manuscript.

Funding: This research received no external funding.

Institutional Review Board Statement: Not applicable.

Informed Consent Statement: Not applicable.

Data Availability Statement: Data are contained within the article.

Acknowledgments: The authors would like to express their gratitude to LLP "International Educational Corporation" for their support and assistance in conducting this research.

Conflicts of Interest: Prof. Aidana Kuanyshbay, Dr. Sayat Niyetbay, Dr. Indira Tashmukhanbetova and Prof. Ruslanzhan Sadyrov were employed by International Educational Corporation. The remaining authors declare that the research was conducted in the absence of any commercial or financial relationships that could be construed as a potential conflict of interest.

References

1. Jelle, B.P.; Gustavsen, A.; Baetens, R. The Path to the High Performance Thermal Building Insulation Materials and Solutions of Tomorrow. *J. Build. Phys.* **2010**, *34*, 99–123. [CrossRef]
2. Apkar'yan, A.S. Investigation of the Density of Granular Foam-Glass Ceramic by Mathematical Modeling. *Glass Ceram.* **2014**, *71*, 194–197. [CrossRef]
3. Fu, F.; Hu, N.; Ye, Y.; Chen, G.; Jia, J. Production of Lightweight Foam Ceramics by Adjusting Sintering Time and Heating Rate. *Constr. Build. Mater.* **2023**, *394*, 132063. [CrossRef]

4. Liang, J.; Tang, Z.; Qi, F.; Jiang, W.; Lao, X.; Miao, L.; Tang, H.; Liu, J.; Bao, Z. Preparation of Foam Ceramics from Solid Wastes: A Study on the Relationship between Firing Regime and Properties by Grey System Theory. *J. Mater. Res. Technol.* **2023**, *26*, 58–70. [CrossRef]
5. Pazouki, M.; Zamani, F.; Khalili, M. Development of Clay Foam Ceramic as a Support for Fungi Immobilization for Biodiesel Production. *Int. J. Eng. Trans. B Appl.* **2014**, *27*, 1691–1696. [CrossRef]
6. Rugele, K.; Lehmhus, D.; Hussainova, I.; Peculevica, J.; Lisnanskis, M.; Shishkin, A. Effect of Fly-Ash Cenospheres on Properties of Clay-Ceramic Syntactic Foams. *Materials* **2017**, *10*, 828. [CrossRef]
7. Headley, A.J.; Hileman, M.B.; Robbins, A.S.; Piekos, E.S.; Stirrup, E.K.; Roberts, C.C. Thermal Conductivity Measurements and Modeling of Ceramic Fiber Insulation Materials. *Int. J. Heat. Mass. Transf.* **2019**, *129*, 1287–1294. [CrossRef]
8. Akbarnejad, S.; Jonsson, L.T.I.; Kennedy, M.W.; Aune, R.E.; Jönsson, P.G. Analysis on Experimental Investigation and Mathematical Modeling of Incompressible Flow Through Ceramic Foam Filters. *Metall. Mater. Trans. B Process Metall. Mater. Process. Sci.* **2016**, *47*, 2229–2243. [CrossRef]
9. Sedlačík, M.; Nguyen, M.; Opravil, T.; Sokolář, R. Preparation and Characterization of Glass-Ceramic Foam from Clay-Rich Waste Diatomaceous Earth. *Materials* **2022**, *15*, 1384. [CrossRef]
10. Odewole, P.O. Properties of Glass-Ceramics Foam Based on Granite Dust-Clay-Maize Cob Composite as a Sustainable Building Material. *J. Sustain. Constr. Mater. Technol.* **2022**, *7*, 1–8. [CrossRef]
11. Dutto, A.; Zanini, M.; Jeoffroy, E.; Tervoort, E.; Mhatre, S.A.; Seibold, Z.B.; Bechthold, M.; Studart, A.R. 3D Printing of Hierarchical Porous Ceramics for Thermal Insulation and Evaporative Cooling. *Adv. Mater. Technol.* **2023**, *8*, 2201109. [CrossRef]
12. Zhou, W.; Yan, W.; Li, N.; Li, Y.; Dai, Y.; Han, B.; Wei, Y. Preparation and Characterization of Mullite Foam Ceramics with Porous Struts from White Clay and Industrial Alumina. *Ceram. Int.* **2018**, *44*, 22950–22956. [CrossRef]
13. Ivanov, K.S. Associated Synthesis of Microgranular Foam-Glass Ceramics from Diatomaceous Clays. *Steklo I Keram.* **2022**, *79*, 234–238. [CrossRef]
14. Huo, W.L.; Zhang, X.; Hu, Z.; Chen, Y.; Wang, Y.; Yang, J. Silica Foams with Ultra-Large Specific Surface Area Structured by Hollow Mesoporous Silica Spheres. *J. Am. Ceram. Soc.* **2019**, *102*, 955–961. [CrossRef]
15. Shang, L.; Wu, D.; Pu, Y.; Wang, H.; Wang, F.; Gao, Z. Experimental Research on Thermal Insulation Performance of Lightweight Ceramic Material in Oxidation Environment up to 1700 °C. *Ceram. Int.* **2016**, *42*, 3351–3360. [CrossRef]
16. Morales, R.D.; Davila-Maldonado, O.; Adams, A.; Oliveira, L.; Alquist, B. Computer and Fluid Flow Modeling of Filtration Mechanisms in Foam Filters. *AFS Trans.* **2008**, *116*, 715–731.
17. Yang, F.; Yao, Y.; Yang, Z.; Zhao, S.; Chen, G.; Li, K. Fabrication of In-Situ Self-Reinforced Si3N4 Ceramic Foams for High-Temperature Thermal Insulation by Protein Foaming Method. *Ceram. Int.* **2021**, *47*, 18351–18357. [CrossRef]
18. Bowen, J.J.; Mooraj, S.; Goodman, J.A.; Peng, S.; Street, D.P.; Roman-Manso, B.; Davidson, E.C.; Martin, K.L.; Rueschhoff, L.M.; Schiffres, S.N.; et al. Hierarchically Porous Ceramics via Direct Writing of Preceramic Polymer-Triblock Copolymer Inks. *Mater. Today* **2022**, *58*, 71–79. [CrossRef]
19. Shiskin, A.; Bumanis, G.; Irtiseva, K.; Ozolins, J.; Korjakins, A. Clay Ceramic Hollow Sphere—Cement Syntactic Foam Composite for Building Applications. *Key Eng. Mater.* **2019**, *800*, 228–234.
20. Ketov, A.; Rudakova, L.; Vaisman, I.; Ketov, I.; Haritonovs, V.; Sahmenko, G. Recycling of Rice Husks Ash for the Preparation of Resistant, Lightweight and Environment-Friendly Fired Bricks. *Constr. Build. Mater.* **2021**, *302*, 124385. [CrossRef]
21. Rashid, M.; Ul Haq, E.; Yousaf, S.; Javed, M.; Nadeem, M.; Aziz, U.; Abbas, A.Q. Light Weight Low Thermal Conductive Fly Ash Foams through Microwave Irradiation for Insulative, Agricultural and Self-Healing Purposes. *Mater. Today Proc.* **2020**, *47*, S38–S45.
22. Kazantseva, L.K.; Rashchenko, S.V. Chemical Processes during Energy-Saving Preparation of Lightweight Ceramics. *J. Am. Ceram. Soc.* **2014**, *97*, 1743–1749. [CrossRef]
23. Shinguzhieva, A.; Kurmaniyazova, N.; Urazova, A.; Satybayeva, N.; Mukhanbetzhanova, K. Influence of Oil Slurry on the Properties of Light Aggregates Based on Loams. *Int. J. Eng. Trends Technol.* **2023**, *71*, 257–266. [CrossRef]
24. Wang, E.; Shi, Z.; Chen, M.; Tang, S.; Zhang, X.; Zhang, W. Investigation of Effective Thermal Conductivity of SiC Foam Ceramics with Various Pore Densities. *Open Phys.* **2022**, *20*, 58–65. [CrossRef]
25. Rumi, M.K.; Urazaeva, E.M.; Mansurova, E.P.; Irmatova, S.K.; Faiziev, S.A.; Zufarov, M.A.; Arushanov, G.M. Preparation of Highly Porous Materials Based on Refractory Clays. *Glass Ceram.* **2020**, *77*, 87–93. [CrossRef]
26. Lin, Z. Tunnel Kiln Stack Firing Method of Foam Ceramic Lightweight Plate. CN208720785U, 9 April 2018.
27. Gonzenbach, U.T.; Studart, A.R.; Steinlin, D.; Tervoort, E.; Gauckler, L.J. Processing of Particle-Stabilized Wet Foams into Porous Ceramics. *J. Am. Ceram. Soc.* **2007**, *90*, 3407–3414. [CrossRef]
28. Ansari, A.I.; Sheikh, N.A. A Review on Different Approaches for Foam Fabrication. *J. Inst. Eng. (India) Ser. C* **2023**, *104*, 1219–1245.
29. Sinitsin, D.A.; Shayakhmetov, U.S.; Rakhimova, O.N.; Khalikov, R.M.; Nedoseko, I.V. Nanostructured Foam Ceramics for Building Purposes: Production Technology and Applications. *Nanotechnol. Constr.* **2021**, *13*, 213–221. [CrossRef]

30. Vakalova, T.V.; Revva, I.B. Highly Porous Building Ceramics Based on «clay-Ash Microspheres» and «zeolite-Ash Microspheres» Mixtures. *Constr. Build. Mater.* **2022**, *317*, 125922. [CrossRef]
31. Liu, W.; Liang, J.; Fu, C.; Zeng, B.; Huang, M.; Yang, G.; Luo, X.; An, D.; Wei, S.; Xie, Z.; et al. Waste Recycling of Coal Fly Ash: A Novel Approach to Prepare Hierarchically Porous Coal Fly Ash/Al_2O_3 Ceramic Composite with High Porosity and High Strength Templated by Emulsion-Assisted Self-Assembly. *Ceram. Int.* **2022**, *48*, 18588–18595. [CrossRef]
32. Barracco, F.; Demichelis, F.; Sharifikolouei, E.; Ferraris, M.; Fino, D.; Tommasi, T. Life Cycle Assessment for the Production of MSWI Fly-Ash Based Porous Glass-Ceramics: Scenarios Based on the Contribution of Silica Sources, Methane Aided, and Energy Recoveries. *Waste Manag.* **2023**, *157*, 301–311. [CrossRef] [PubMed]
33. Ketov, A.; Korotaev, V.; Rudakova, L.; Vaisman, I.; Barbieri, L.; Lancellotti, I. Amorphous Silica Wastes for Reusing in Highly Porous Ceramics. *Int. J. Appl. Ceram. Technol.* **2021**, *18*, 394–404. [CrossRef]
34. Mangutova, B.; Fidancevska, E.; Milosevski, M.; Bossert, J. Production of Highly Porous Glass-Ceramics from Metallurgical Slag, Fly Ash and Waste Glass. *Acta Period. Technol.* **2004**, *50*, 103–110. [CrossRef]
35. An, L.; Armstrong, J.N.; Hu, Y.; Huang, Y.; Li, Z.; Zhao, D.; Sokolow, J.; Guo, Z.; Zhou, C.; Ren, S. High Temperature Ceramic Thermal Insulation Material. *Nano Res.* **2022**, *15*, 6662–6669. [CrossRef]
36. Bessimbayev, Y.T.; Niyetbay, S.E.; Awwad, T.; Kuldeyev, E.I.; Uderbayev, S.S.; Zhumadilova, Z.O.; Zhambakina, Z.M. The Creation of Geotechnical Seismic Isolation from Materials with Damping Properties for the Protection of Architectural Monuments. *Buildings* **2024**, *14*, 1572. [CrossRef]
37. Sahoo, S.K.; Shrivastava, U.; Khan, M.Z. Thermal Insulation Ceramic Material by Using Coal Combustion Waste Fly Ash and Waste Glass with Medicinal Phytochemical Repellent. In *IOP Conference Series: Materials Science and Engineering*; IOP Publishing Ltd.: Bristol, UK, 2020; Volume 798.
38. Wang, C.; Xu, G.; Gu, X.; Gao, Y.; Zhao, P. High Value-Added Applications of Coal Fly Ash in the Form of Porous Materials: A Review. *Ceram. Int.* **2021**, *47*, 22302–22315.
39. Zhu, M.; Ji, R.; Li, Z.; Wang, H.; Liu, L.L.; Zhang, Z. Preparation of Glass Ceramic Foams for Thermal Insulation Applications from Coal Fly Ash and Waste Glass. *Constr. Build. Mater.* **2016**, *112*, 398–405. [CrossRef]
40. *GOST 32026–2012*; Raw Clay Materials for the Production of Expanded Clay Gravel, Crushed Stone and Sand. Interstate Standard. Approved by the Order of the Federal Agency for Technical Regulation and Metrology No. 1981-st of December 27, 2012. Ef-fective from January 1, 2014 (in Russian). Russian GOST: St. Petersburg, Russia, 2012. Available online: https://meganorm.ru/Data2/1/4293780/4293780349.pdf (accessed on 21 February 2025).

Disclaimer/Publisher's Note: The statements, opinions and data contained in all publications are solely those of the individual author(s) and contributor(s) and not of MDPI and/or the editor(s). MDPI and/or the editor(s) disclaim responsibility for any injury to people or property resulting from any ideas, methods, instructions or products referred to in the content.